

Neuromorphic Artificial Vision Systems Based on Reconfigurable Ion-modulated Memtransistors

zhen yang (Peking University)¹, Teng zhang (Peking University)¹, Keqin Liu (Peking University)¹, Bingjie Dang (Peking University)¹, Liying Xu (Peking University)¹, Yuchao Yang (Peking University)¹, and Ru Huang (Peking University)¹

¹Affiliation not available

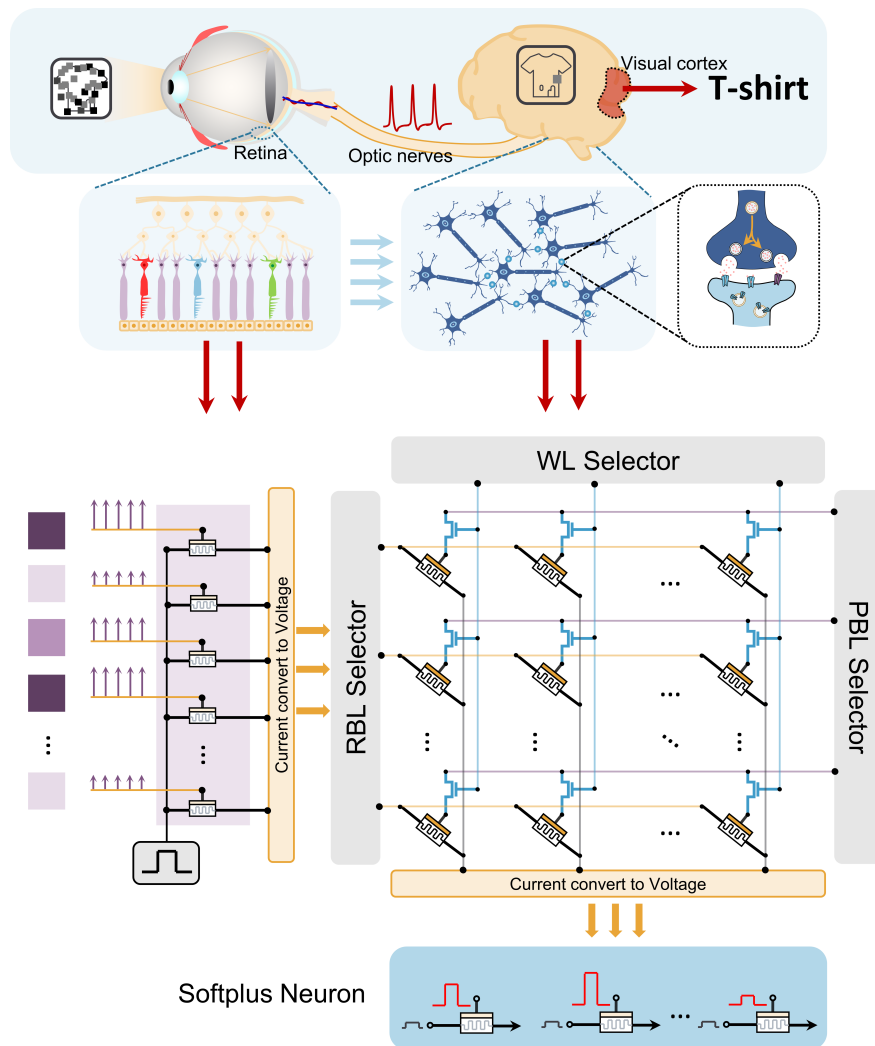
March 21, 2023

Abstract

Conventional vision systems suffer from lots of data handling between memory and processing units. Inspired by how humans recognize noisy images and the flexible modulation on the timescale of ion dynamics inside an emerging memtransistor, we report a novel neuromorphic vision system based on the ion-modulated memtransistors. By controlling the ion doping processes under adequate stimuli strengths, both short-term and long-term ion dynamics can be utilized to deliver energy-efficient data processing. When dealing with image reconstructions, the short-term accumulation effect of the device can help filter noises in a set of received noisy images while enhancing the original pattern information. The increased contrast can help distinguish the actual contents. To demonstrate systematic performances with the reconfiguration of devices, we extract the nonlinear relationship between channel conductance variation and the amplitude of gate pulses into the network-level simulation. Also, with the nonvolatile conductance change characteristic, the task of recognizing noisy images is performed to verify the versatility of ion-modulated memtransistors in the neuromorphic artificial vision systems.

Corresponding author(s) Email: tengzhang@pku.edu.cn yuchaoyang@pku.edu.cn

ToC Figure



Inspired by how humans recognize noisy images and flexible modulation on the timescale of ion dynamics, we proposed a novel neuromorphic vision system based on the ion-modulated memtransistors. By utilizing the reconfiguration abilities, which include nonvolatile conductance change characteristics and short-term filtering or nonlinear activation, the task of recognizing noisy images can be performed in a more energy-efficient manner.

Introduction

In the past few decades, computer vision (CV) has achieved considerable progress with advanced intelligent algorithms and computing hardware.^[1-3] However, most image-data-based processing algorithms require a large number of parameters that are usually stored in the memory module, which will cause frequent data transfer between memory and processor when the systems receive sensor information.^[4, 5] Inspired by the in-memory computing feature in the human brain and combined with modern deep neural networks (DNN), the crossbar arrays made of emerging nonvolatile memories (eNVM) are implemented to accelerate the multiply-

accumulate (MAC) operations which dominated mostly in DNN.^[6-10, 37] In addition to the synaptic devices exploration, recently, as also the core components of neuromorphic computing, there was plenty of research about searching for the hardware implementation of neurons based on emerging materials and devices.^[11-14] For instance, the memristive neurons, including Mott memristors,^[15-19] redox memristors,^[20, 21] phase-change memristors,^[22] etc, all of them can emulate the leaky integrate-and-fire (LIF) function of biological neurons.

However, the device type and materials between the hardware implementation of synapses and neurons usually differ from each other, which will cause additional fabrication costs in large-scale integration and severe limits on the scalability for further applications.^[15, 21] Nowadays, many researchers put forward the idea of reconfiguring device's functions on the same hardware platform.^[14, 23-25] One of the studies made use of reconfigurable synaptic and neuronal functions in the V/VO_x/HfWO_x/Pt memristors for spiking neural network,^[23] manipulating the ion distributions in HfWO_x memristors to enable devices working on different modes.

Moreover, inspired by how neurotransmitters modulate human neural networks, investigators tend to exploit moveable ions, such as H⁺, Li⁺ and O²⁻,^[24, 26-30] to regulate the electrical properties of materials, which has made neuromorphic hardware advance a big step. For instance, by changing the local distribution of hydrogen ions, researchers have demonstrated the reconfigurable perovskite nickelate electronics for reservoir computing and incremental learning.^[24]

In a complete neuromorphic system, it is also critical to pre-process external information after sensing from the outside world. Most of the information humans receive is obtained through vision, simulating the vision systems of humans is of great importance to the artificial perception system.^[31] There were also many explorations about building an artificial vision system to process the data correlated with vision. However, little effort had been devoted to combining the reconfiguration ideas with energy-efficient neuromorphic vision systems, which can help reduce complexity of the system.

Inspired by ionic regulation methods and reconfiguring advantages, we propose an energy-efficient vision system based on reconfigurable ion-modulated memtransistors. With different stimuli ranges, the temporal scales of ion dynamics inside the devices can be well controlled. As for the short-term dynamics, the accumulation effect can help filter the random noises and enhance the original patterns simultaneously, which was demonstrated in the reconstruction from a set of noisy images. After that, we investigate the relationship between the channel conductance changes and stimuli amplitudes. The observed nonlinear relation can both be used for softplus-like neurons and filtering units. By changing external stimuli, long-term channel conductance modulation can also be achieved to implement weight storage. Based on the above considerations, we present an architecture for neuromorphic vision systems based on the reconfigurable ion-modulated memtransistors. In the system-level performance demonstration, an artificial neural network (ANN) was implemented to recognize the Fashion-MNIST datasets where the filtering units, synapse weights and activation neurons were all based on the ion-modulated memtransistors. Through detailed analysis and testing of the mapping strategies and noises on the network-level performances, we prove that the neuromorphic vision system can help recognize images in practice with relatively high accuracy and improved robustness.

2. Results and Discussion

2.1. Brain-inspired visual processing system based on ion-modulated memtransistor.

According to the experiments conducted by Treichler,^[32] 83% of the information received by human come from vision, so the visual system plays a crucial role in the perception of the human brain. **Figure 1** a shows conventional image recognition systems, which mainly include the sensor array, memory module, computing unit (e.g., CPU) and post-processing unit (e.g., GPU). First, raw image data are received by the sensor chip, and then the sensor data get stored in the memory devices for subsequent processing. Due to the more-or-less influences caused by the environmental change, the raw data generally carry some noise, so the denoising algorithm is deployed in the computing unit. Massive data are transferred between computing units and memory devices before the algorithm converges. After that, the pre-processed images are sent to the post-

processing units, which perform the final classification based on the neural network algorithm. Similar to the data transfer between pre-processing units and memory devices, the neural network parameters are mainly stored in the memory module. Plenty of data need to be transferred frequently between the post-processing units and memory module when implementing the inference.

Given the large amount of data handling, the delay and power consumption get much increased for the conventional image recognition system. Introducing some denoising algorithms also increases the computational complexity of the whole system. For human visual systems, the identification of noisy images is rapid and accurate. Figure 1b presents the human visual system. External information is delivered to the retina of the human eye, then the rod cells and cone cells in the retina integrate the original information. This integrated information is transmitted through the optic nerve to the visual center of the brain. After computing in the network of neuronal cells located in the cerebral cortex, the concrete images were finally identified.

Compared with traditional hardware visual recognition systems, human visual systems are more tolerant of errors, while processing complexity and energy consumption are both at ultra-low levels. Inspired by that, we propose an artificial visual system based on reconfigurable ion-modulated memtransistors (Figure 1c) by limiting the range of signal strength applied to the gate, which enables the device to act as the key parts for different modules. These different modules mainly include 1) filtration units that simulate the function of cells on the retina which execute the information pre-processing; 2) accelerating the in-memory computing unit of the matrix-vector multiplication (MVM) used for image classification inference. And 3) nonlinear activation of neurons after receiving synaptic weighted calculations. By elaborately utilizing ion dynamics with different temporal scales which can be controlled inside the device, image recognition can be implemented more efficiently and reliably.

2.2. Tunable ion dynamics and plasticity of the ion-modulated memtransistors

Figure 2 a shows a schematic diagram of an ion-modulated memtransistor, in which amorphous NbO_x acts as the channel material. As a strongly correlated transition metal oxide, NbO_x has an intrinsic low conductance level and sensitivity to ion doping, allowing the system to be easily modulated under ion doping with lower power consumption.^[33-36] Figure 2b shows the top view of the device under an optical microscope and the cross-sectional transmission electron microscope (TEM) images can be seen in Figure 2c. The detailed process of device fabrication is presented in the Experimental Section. The spatial mapping of dominant elements using energy-dispersive X-ray spectroscopy (EDS) is shown in Figure 2d, including O, P, N, Nb, Si, Ti and Au elements. Also, an EDS line scan through the red arrow in Figure 2d is conducted, which is illustrated in Figure 2e. To fabricate the amorphous LiPON ion conductor, the Li_3PO_4 target was deposited by the RF magnetron sputtering under N_2 flow of 10 sccm, where the reaction between Li_3PO_4 and N_2 will happen, enabling nitrogen atoms to get into the Li_3PO_4 to form LiPON. In the element characterization, we can see that nitrogen elements are evenly dispersed within the electrolyte layer, forming an amorphous LiPON fast ion conductor. Specific doping modification processes can be seen in Figure 2f. With the introduction of nitrogen atoms into the initial lithium phosphate crystals, the oxygen atoms in the original lattice will be replaced, including both bridge oxygen atoms and non-bridge oxygen atoms, so that the reticular crosslinking structure in the system increases significantly and enable lithium ions to move more easily in the electrolyte.

To measure the memory effect of the ion-modulated memtransistor, forth and back sweeps were conducted on gate bias from -6 V to 4 V, with the small drain-source voltage kept at 0.1 V, anticlockwise hysteresis for the channel current can be observed in Figure 2g, the average on/off ration at 0 V gate bias for the thirty sweeps is approximately 125. The insets in Figure 2g show the ion dynamics while under different stimuli ranges, as Li ions in the LiPON electrolyte are driven to approach or get away from the interface between the electrolyte and the channel under the positive or negative gate bias, which could reversibly modulate the channel conductance. For instance, under the positive gate bias, the electric field will drive the cationic Li ions to migrate to the channel interface, which can form the electric double layer; if under the strong electric field, the moved ions maybe intercalate the deficient sites within the amorphous NbO_x , the electrochemical reaction will take place in that, which will lead the reduction of Nb^{5+} to Nb^{4+} and the generation for the

extra defect energy level. The different sites for the Li ions gathered with respect to the channel correspond to different ionic temporal dynamics, which will be explored in the following experiments. Figure 2h collects the statistical drain current at the on-state or off-state for 0 V gate bias, and both fluctuations are at relatively lower levels. Also, as shown in Figure 2i, the gate leakage current is limited under the sub-nA, which keeps the programming energy ultra-low. Figure 2j and 2k present the transfer curves at different dynamic ranges and sweeping rates, respectively, and the corresponding gate leakage current can be seen in Figure S1 and S2, Supporting Information, as the larger sweeping bias and slower sweeping rate can induce the more prominent increase of the drain-source current.

To explore the relationship between the amplitude of the gate bias and the temporal scale of ion dynamics, a train of gate pulses with different amplitudes (1 V to 5 V) was applied while keeping both the pulse width and interval at 100 ms. As shown in **Figure 3 a**, increased amplitudes raise more significant channel current and the changes are more likely to be retained after the gate pulses removing, which implies that the memory effect transferred from short-term to long-term. To investigate the short-term memory effect, different pulse widths with fixed amplitude at 2 V, and different pulse amplitudes with fixed widths at 200 ms were applied to the device. The results are shown in Figures 3b and 3c, with more intense stimuli, the channel current reaches a higher level. In addition to the single pulse testing, we also applied a pair of positive pulses with different intervals on the gate to explore the paired-pulse facilitation (PPF) effect of the ion-modulated memtransistor. As illustrated in Figure 3d, the accumulative effect is represented by the ratio of the peaks of drain-source current change induced by the applied pulse pairs (PPF ratio), the relevance between the PPF ratio can be described by a double exponential decay function: $1+C_1e^{-\Delta\tau/\tau^1}+C_2e^{-\Delta\tau/\tau^2}$, the two time constants after fitting are 999.78 ms and 163.62 ms respectively. Similarly, spike-rate-dependent plasticity (SRDP) was investigated in Figure 3e, ten pulses with frequencies of 25, 10, 5, 2 and 1 Hz (2.5 V, 100 ms) were applied to the device, and a more substantial cumulative effect could be observed in the pulse train with higher frequency.

As for long-term ion dynamics investigation, as shown in Figure 3f, different numbers of more strong pulse stimuli (5 V, 200 ms) were applied, and the channel current was continuously monitored by the constant small bias (0.2 V) at the drain side. It can be seen that the channel current change could be retained under strong stimuli, which is different from that channel current decaying back to the initial state in the short-term memory. In Figure 3g, we fixed the number of strong gate pulses while varying the amplitude, and the final retained channel current change could be more prominent under the larger gate pulses. In Figure 3h, eight distinguished states were selected to test their retention for 100 s after the removal of gate pulses with 0.2 V bias applied on the drain terminal. To quantitative describe the device state retention ability, we define a coefficient by the relative drain-source current change concerning the initial level between the current at 0 s and 100 s and all the coefficients about the current change maintained at the lower level. Besides, longer duration of channel conductance of two states with a ratio of 60 was measured, which is shown in Figure 3i. Then 50 distinguished states were shown in Figure 3j, implying that the device state can be tuned to much more levels. And the long-term channel conductance modulation by the gate pulse is shown in Figure 3k, 50 identical positive and negative gate pulses (8 V/-6 V, 100 ms) and 10 cycles of bidirectional analog switching were sequentially applied, and 50-level reproducible switching can be achieved.

The above results show that ion-modulated memtransistors both possess short-term and long-term ion dynamics and can be modulated flexibly by adjusting the amplitude of stimuli, which makes the devices vital blocks for different parts of the artificial neuromorphic vision systems.

2.3. Image reconstructions through short-term accumulations of the ion-modulated memtransistors

For human beings, identifying and reconstructing the original images from a series of noisy images is simple and fast, as shown in Figure 4a. It is difficult to identify the original images from each of these series alone. However, it is easier to identify them once they are presented subsequently, which gives inspiration that we can take advantage of the short-term memory features of the devices to extract the real content behind a series of disturbing images. First, we convert the pixel values of different time points corresponding to the

same location of the images into electrical pulses, using binary images and four different time points for the convenience of testing, as shown on the right of Figure 4b. After that, the converted electrical pulses were applied to the gate of the devices with 0.2 V drain-source bias for reading. Pixel values 1 and 0 correspond to pulse amplitude values of 3 V and 0 V respectively while keeping the width at 100 ms and the period at 150 ms. A combination of spatio-temporal information corresponding to the final drain-source current was summarized in the left of Figure 4b. The three patterns corresponding to the letters ‘X’, ‘Y’ and ‘Z’ with some random noises added manually, which makes it hard to identify exactly which letter of each image among them. Then these converted electrical pulses were fed into the ion-modulated-memtransistors-based array according to the previous spatiotemporal information encoding scheme, as schematically depicted in Figure 4c. Detailed encodings for each letter can be found in Figure S3, Supporting information. Finally, the resulting channel current changes are summarized, as shown in Figure 4d. The specific current variation for each pixel can be found in Figure S4, S5 and S6, Supporting Information. The reconstructed images can show the original letter patterns more clearly, implying that the original feature information with extra noises can be accumulated and filtered at the same time, the signal-to-noise ratio can be improved and the original factual information then can be recognized.

2.4. Full-hardware neuromorphic vision system based on reconfigurable ion-modulated memtransistors

Since the directional movement of ions in the electrolyte needs to surmount potential energy barrier, and the additional silicon oxide layer also causes an inevitable voltage drop, the short-term response of the device has a nonlinear relationship with the amplitude of external stimuli. To investigate the nonlinear response, we applied a series of identical pulses to the device, ranging in amplitudes from 0.2 V to 3.6 V. The corresponding increases in drain current were shown in Figure 5a. The drain current at the end of the last stimuli pulse and the first pulse stimuli were summarized in Figure 5b and 5c, respectively. To take the relation between the drain current responses and stimuli amplitude into systematic computation, a softplus-like function ($y = \text{aln}(1 + e^{bx})$) was adopted to fit the experimental results.

In artificial vision system, images captured by image sensor are often distorted by various noises, such as electrical noise, mechanical noise, channel noise and other noises, during generation and transmission. To suppress noise, improve image quality, and facilitate higher-level processing, image denoising is performed using the short-term dynamics of the ion-modulated memtransistors, as illustrated in the inset of Figure 5b. During inference, the MVM is often performed by applying a short pulse on the bit line. We use the channel current change characteristic after the single-pulse stimulus in the operation of neuron activation in the inference, which is shown in the inset of Figure 5c. The schematic of the basic neural network architecture for the neuromorphic vision system is demonstrated in Figure 5d, mainly including filtering units for denoising, synapses for MVM and hardware softplus neurons for nonlinear activation. Then the artificial neuromorphic hardware systems for visual information processing were proposed based on the ion-modulated memtransistors, as shown in Figure 5e. After stimulating by the encoded electrical pulses in the filtering units, the drain currents were transferred into voltage pulses in a linear mapping relation. Then the converted voltage pulses were fed into the Computing-in-Memory array to perform MVM. The basic cell consists of one transistor and one ion-modulated memtransistor (1T1M), in which the transistor is responsible for selective programming and retention enhancing. Finally, the cumulative current after the MVM is converted to voltage pulses and then applied on the gate to utilize the softplus-like response to achieve the nonlinear activation.

As shown in **Figure 6 a**, we simulated multilayer perception (MLP, inset in Figure 6a) for the evaluation of the network-level performance using the ion-modulated memtransistor for softplus neurons. The simulation details can be found in the Experimental Section, there was almost no difference in the testing accuracy between the standard software softplus neuron and the hardware softplus neuron. Unlike weight updating, there is supposed to be no accumulation in the device state for the application of neuron function. To avoid the transition between short-term memory and long-term memory, it is necessary to impose a constraint on the amplitude of gate pulses. We define the viable upper limit amplitude of the gate pulses as cutoff voltage,

with minimizing the cutoff voltage, the accumulative effect can be overcome and programming energy can be saved. As shown in Figure 6b and 6c, there is no significant difference in the network performance with cutoff voltage in the interval between 3.0 V and 3.5 V. However, a noticeable degradation took place when the cutoff voltage reached 2.9 V. Moreover, after reducing the cutoff voltage below 2.8 V, there is no classification ability for the neural network, with the accuracy all about 10%. After investigating the adequate upper limit of gate pulses, we set the cutoff voltage as 3 V. To characterize the endurance of the devices, a train of pulses of 3 V was applied on the device gate. Figure 6d shows no sign of ON/OFF ratio degradation up to 2000 cycles, implying that there is no need to reset the device to the initial state with the help of peripheral circuits. The spontaneous decaying characteristic can ensure repeated activations in the inference. As for the noisy nature of the diffusion of the random ions, we explore the influence on the neural network performance under the noise of the hardware softplus neuron. It can be seen in Figure 6e that the neural network can tolerate the considerable noise level of the hardware softplus neuron, implying the robustness for the ion-modulated memtransistor configuring as the neuron function, the hardware softplus functions with Gaussian noise of different standard deviation were also compared in Figure S7a, Supporting Information, and the collection of testing accuracies for the network concerning the neuron function was demonstrated in Figure S7b, Supporting Information.

Following the discussions about hardware softplus neuron implementation, we choose the cutoff voltage of 3 V and noise level of 10% for the subsequent investigation of the filtering function of ion-modulated memtransistors. Firstly, we compared the same images in three different states: 1) Original; 2) With 10% Gaussian noise; 3) After softplus-like function filtering; and the results are shown in Figure 6f. Compared with the noisy images, after filtering, background noises could be suppressed and critical image information got enhanced. Although there was an overall reduction in the specific pixel value, the shape could still be distinguished by the enhanced contrast with the background noises. As shown in Figure 6g, after filtering by the device nonlinearity, the testing accuracy got a significant increase from 11.66% to 77.96%, and the corresponding confusion matrix in Figure 6h demonstrated improved classification accuracy by filtering the image noises. One of the determining factors of the specific filtering function is the mapping gate voltage range. As illustrated in Figure S8, Supporting Information, there are some differences among the filtering functions of different starting mapping gate voltages. As shown in Figure 6i, the suitable range of the starting mapping gate voltages was located between 1.5 V and 1.8 V. In the following investigations, the filtering function started mapping from 1.5 V and ended at 3 V. Moreover, one of the typical testing images with different levels of Gaussian noises was demonstrated in Figure 6j, and the final testing accuracies among the original images, noisy images and filtered images were compared in Figure 6k, implying the neuromorphic vision systems can process images with considerable noises which is even hard for the human being to recognize. Finally, we also discussed the impact of different drain biases on device performances. As shown in Figure S9, Supporting Information, with the increase of drain biases, the decaying speed also got boosted, but there were no notable differences in the decaying characteristics when the biases were beyond 0.3 V. Although increased decaying speed can help reduce the delay in the inference, as shown in Figure S10, Supporting Information, the drain current also got increased with the higher drain bias, which will cause extra energy costs for computing. Therefore, final drain bias was set at 0.2 V for tackling the dilemma.

3. Conclusion

We have reported a novel memtransistor of which the channel conductance can be modulated by the ions doping and dedoping under the electric field driving. By adjusting the amplitude of the gate stimuli, both short-term and long-term memory can be realized. Short-term memory effect, such as PPF, SRDP and single pulse stimuli parameters were investigated. Retention, multi-states, LTP and LTD were also acquired to exploit the long-term ion dynamics. By using the short-term accumulation effect, we implemented pattern reconstruction from a set of noisy images. Owing to the energy barrier for ions moving and the inevitable voltage drop on the passivation layer, nonlinear short-term responses can be utilized for hardware softplus neurons and filtering units. By reconfiguring the temporal scales of ion-modulated memtransistor, we proposed an artificial neuromorphic vision system in which filtering units, synapses and activation neurons were constructed with the memtransistors. Moreover, we performed system-level simulations of hardware

neural networks with the ion-modulated memtransistors. All the experimental and simulation results suggest the proposed ion-modulated memtransistor can reduce the delay and energy cost in classifying the noisy images, and thus provides an energy efficient way to construct neuromorphic artificial vision systems.

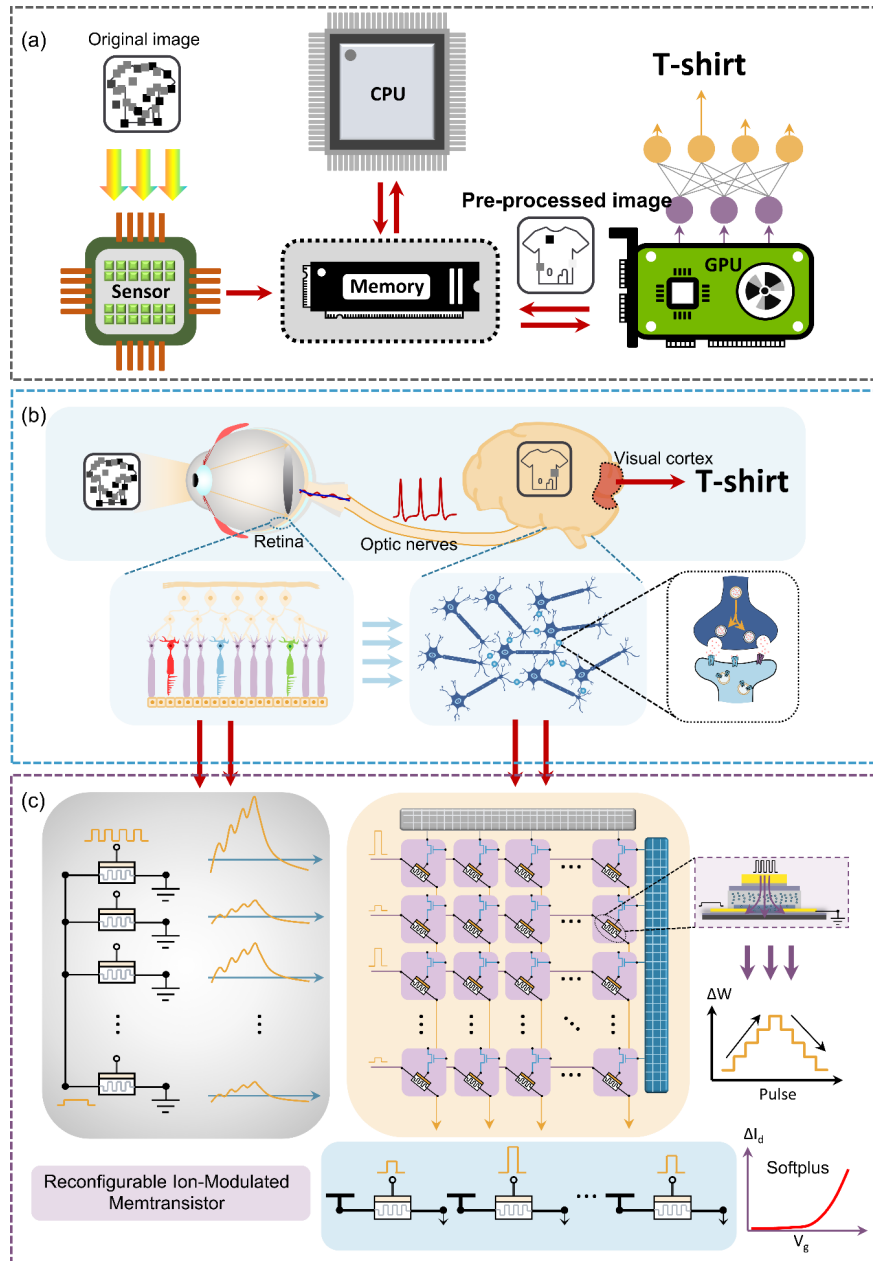


Figure 1. An artificial vision system based on reconfigurable ion-modulated memtransistors inspired by the human visual recognition system. a) Schematic diagram of the conventional image recognition systems, including image denoising and classification algorithm running on the processors. b) Schematic illustration of the human visual system, the optic nerve fibers transmit impulses to the visual cortex when receiving stimulus at the retina from images of the outside world. c) Proposed neuromorphic artificial vision systems based on the reconfigurable ion-modulated memtransistors, which can act as filtering units, in-memory inference

weights and activation neurons simultaneously.

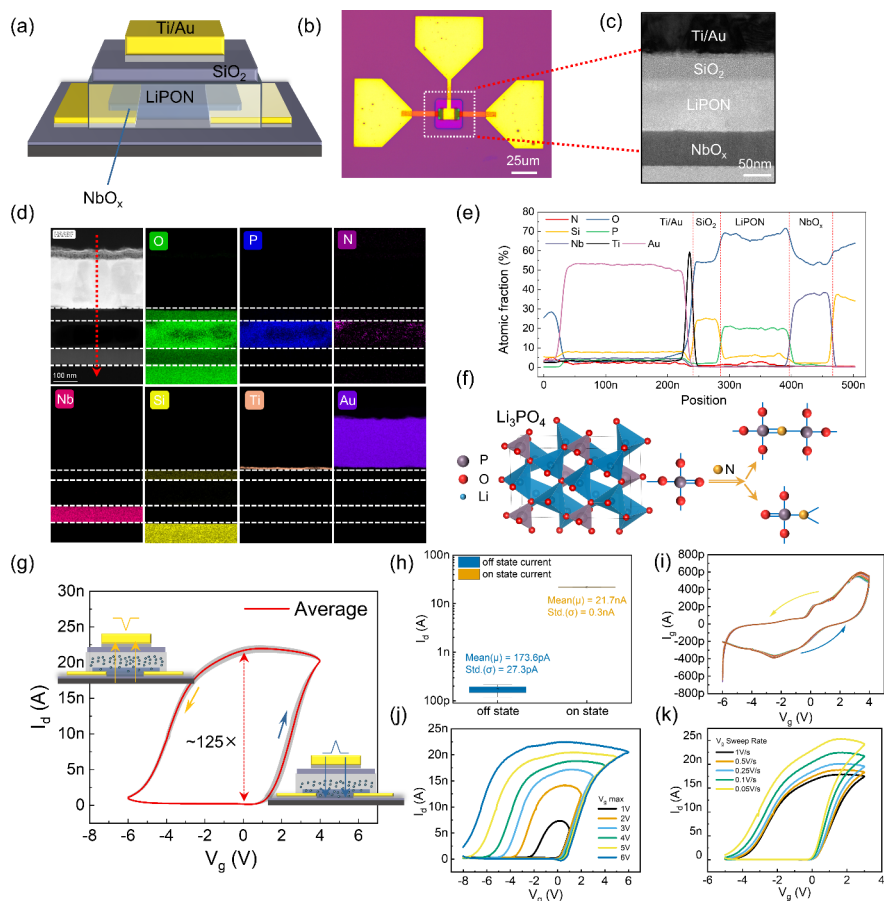


Figure 2. Material characterization and basic DC electrical measurements of the ion-modulated memtransistor. a) Schematic of the ion-modulated memtransistor structure, the channel and solid-state electrolyte are composed of niobium oxide (NbO_x) and lithium phosphorous oxynitride (LiPON), respectively, and silicon oxide act as the passivation layer to keep the electrolyte from oxygen and moisture. b) Optical microscope of ion-modulated memtransistor. c) the cross-sectional TEM image of the central part within the device. d) Elemental mapping of the materials in the device for O, P, N, Nb, Si, Ti, and Au, respectively. e) The line scan EDS of the device cross-section, which corresponds to the red arrow in d). f) Crystal structure of lithium phosphate is composed mainly of $(\text{PO}_4)^{3-}$ tetrahedrons, and lithium ions that are closely bonded to oxygen atoms. In the right part, the P-N and P=N bonds are formed when the nitrogen atoms are doped in $\text{Li}(\text{PO}_4)_3$ crystal. g) Transfer curves of the ion-modulated memtransistor with gate bias swept from -6 V to 4 V at the sweeping rate of 0.53 V/s, which exhibiting counterclockwise hysteresis and the average on/off ratio at 0 V gate bias is approximately 125, the corresponding drain current I_d is monitored by applying small 0.1 V DC bias at the drain terminal. The grey lines represent the results of thirty continuous DC sweeps, and the red line represents the average value of these curves. h) Statistical data of drain current I_d at the on-state or off-state within thirty DC cycles. i) Leakage currents (I_g) variation corresponding to the DC sweeps in g) show the maximum is below 800 pA, which can help reduce energy cost when programming the device. Transfer curves at different sweeping dynamic ranges. j) and sweeping rate k), the drain-source bias is still kept at 0.1 V.

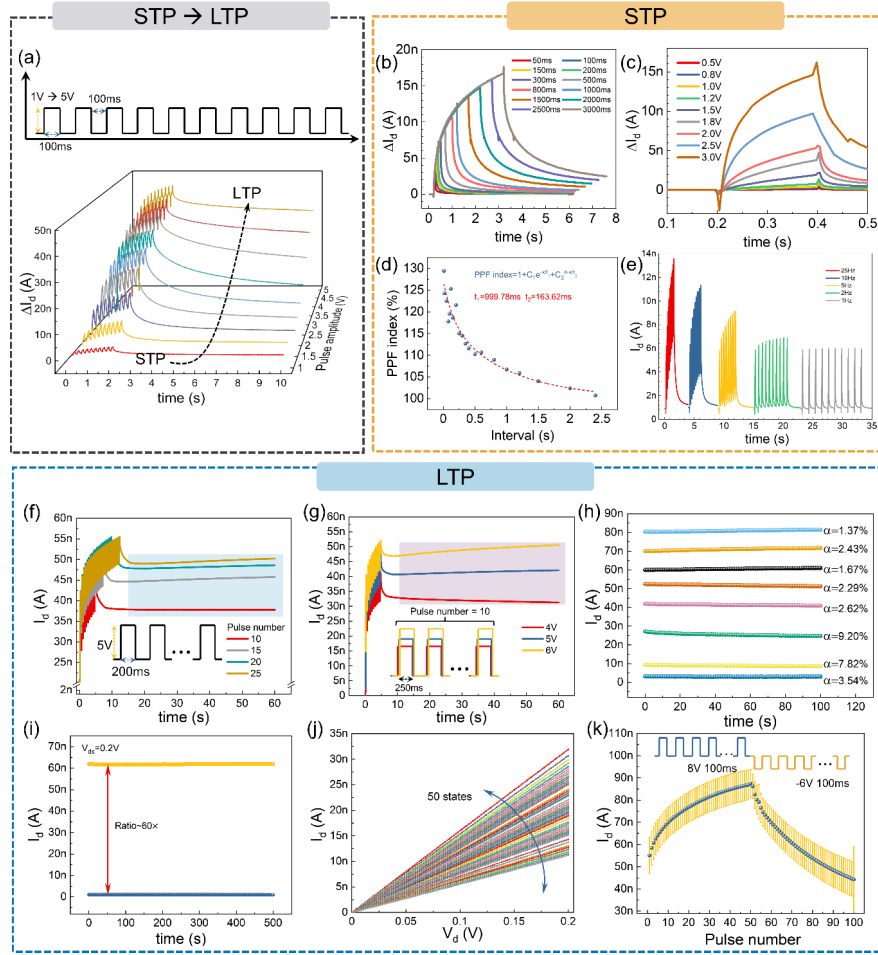


Figure 3. The reconfigurable short-term and long-term ion dynamics with different ranges of stimulus at the gate terminal. a) The rise of drain current (ΔI_d) induced by a chain of ten consecutive pulses, with amplitude ranging from 1 V to 5 V, which shows the conductance change changing from short term to long term. ΔI_d triggered by pulses of different widths b) and amplitudes c) were also conducted to evaluate the short-term ion dynamics in the ion-modulated memtransistors. d) PPF index as a double-exponential decay function of the interval between two pulses, and the red line revealed the fitting results. e) Drain current concerning different pulse frequencies from 1 Hz to 25 Hz, illustrating that the higher stimuli generate more prominent channel current enhancement. To explore the long-term ion dynamics, the relationship between the final drain current of the number f) or considerable amplitude g) of applied pulses is shown. h) Retention performance of eight states of the memtransistor was recorded for 100 seconds. The relative change of conductance is defined as the difference between the initial conductance and final conductance of the device concerning the initial conductance. i) To test the conductance maintenance capacity in longer time scales, two of the many states were selected to perform that. j) Fifty distinguished states were picked to show the analog characteristic of ion-modulated memtransistor. k) Analog states update in both potentiation and depression is shown with 50 pulses of 8 V and -6 V, in which widths were both set at 100 ms. Data are collected from 10 cycles of the LTP and LTD updates.

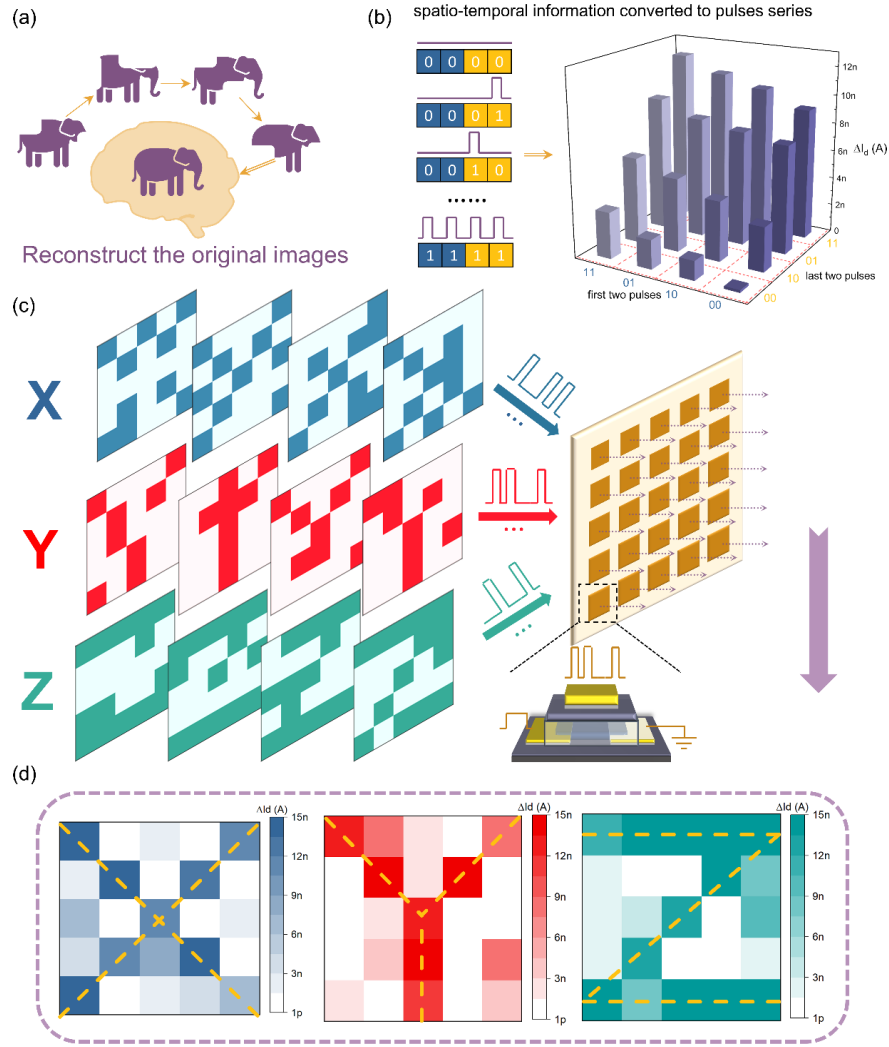


Figure 4. Image reconstructed through the accumulative effect of short-term ion dynamics. a) Schematic of image reconstructing process through a set of images with random noises added on the original image by the human brain. b) Different channel current changes induced by the encoded pulse train of spatiotemporal information. c) A series of pictures with random noise in contrast with the original image was sent to the array continuously, in which the array consisted of ion-modulated memtransistors. d) Experimental results of images reconstructed through the short-term ion dynamics, where the drain current at the end of stimuli represents the value for each pixel.

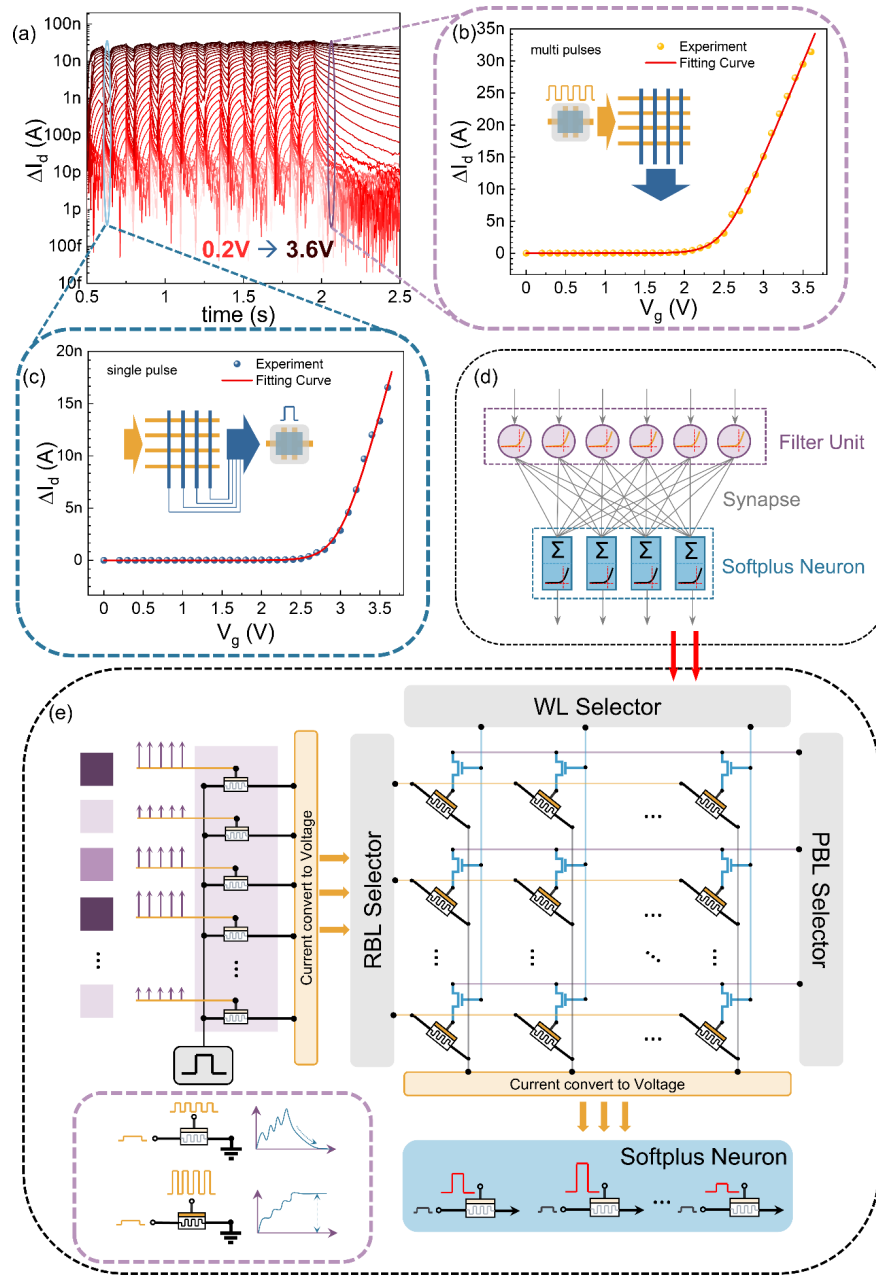


Figure 5. Ion-modulated memtransistors reconfigured as different parts of the neuromorphic vision systems. a) The drain current increases under a train of different amplitudes of gate pulses (from 0.2 V to 3.6 V, 100 ms width and 50 ms interval). b) The drain current at the end of the last stimuli pulse as regards the pulse amplitude, inset shows this relation can be harnessed in filtering image noises. c) The drain current at the end of the first stimuli pulse with respect to the pulse amplitude, inset shows this characteristic can be utilized in the nonlinear activation function. d) The schematic of fundamental neural network architecture, including filtering units, synapses and softplus neurons. e) The hardware systems based on the ion-modulated memtransistors. The different temporal scales of ion dynamics were utilized in different key parts of this neuromorphic vision system.

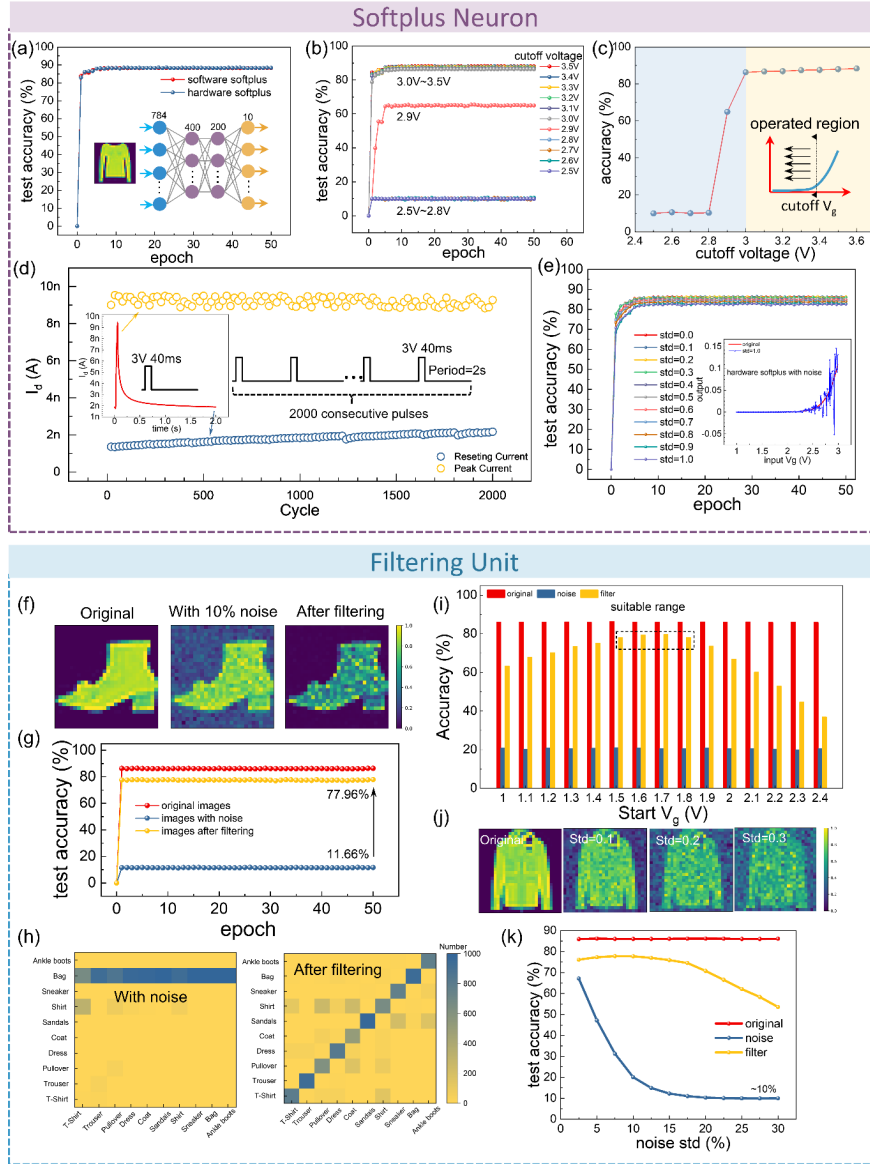


Figure 6. The systematic simulation results for the hardware softplus neuron and filtering unit utilization in the neural network. a) Evolution of the testing accuracy with training epoch between software softplus neuron and hardware softplus neuron applied in the multilayer perceptron (MLP), and main parameters of this MLP are shown in the inset. b) The neural network performances of different cutoff voltages of the hardware softplus neuron. c) The summary of the final testing accuracy for the cutoff voltage, the inset shows the operated region under the constraint of cutoff voltage. d) Endurance testing of the ion-modulated memtransistor as hardware softplus neuron, the peak current and the resting current during pulse stimuli (3 V, 40 ms) were recorded for 2000 cycles. The drain current change under the single gate pulse was shown in the inset. e) The investigation of the testing accuracies concerning the different-level noises on the hardware softplus neuron and the hardware softplus neuron function with Gaussian noise of standard deviation of 1.0 is depicted in the inset. f) The comparison among randomly selected images at the original state after adding 10% Gaussian noise and after filtering by the nonlinearity of the device. g) The testing accuracies evolution for the original images, noisy images and filtered images. h) The confusion matrix for the Fashion-Mnist

classification results for the images with 10% Gaussian noise and after filtering the noises, respectively. i) Final recognition accuracies for different mapping strategies of different starting operation voltages applied at the gate, comparing among the original images, noisy images and filtered images. j) One of the testing images with different levels of Gaussian noises (std=10%, 20%, 30%). k) Testing accuracies among the original images, noisy images and filtered images regarding the standard deviations ranging from 2.5% to 30%.

4. Experimental Section

Fabrication of ion-modulated memtransistor : The ion-modulated memtransistors were fabricated on SiO₂ substrates. First, 5 nm Ti and 25 nm Au were deposited on the substrate through electron-beam evaporation, in which electron-beam lithography was used for patterning. After the source-drain electrode was formed by the lift-off process, the second electron-beam lithography process was carried out to pattern the channel region in the size of 10 um 10 um, then 60 nm NbO_x was deposited on the source-drain contact by magnetron sputtering followed by the lift-off process to form the channel. After that, 120 nm LiPON and 50 nm SiO₂ were prepared by magnetron sputtering as the electrolyte and passivation layer followed by the third electron-beam lithography process. After sputtering was done, the lift-off process was utilized to remove excess material. Finally, after the fourth electron-beam lithography process, 10 nm Ti and 220 nm Au were deposited using electron-beam evaporation. After the last lift-off process, the pads for all the terminals of this device were all completed.

Material characterization : To analyze the material component of the ion-modulated transistors, the TEM samples were prepared firstly by the focus ion beam (FIB) technique (Helios G5 UX). After that, TEM, as well as EDS tests were performed on Talos F200X G2 systems.

Electrical Measurements : All the electrical measurements were performed using an Agilent B1500A semiconductor parameter analyzer. In the pulse testing part, the pulse signal was applied on the gate electrode while the drain-source channel was always under 0.2 V bias.

Simulations : To demonstrate the neuromorphic artificial vision systems based on ion-modulated memtransistors, we adopt the multilayer perceptrons model with the structure of 784-400-200-10, and the Fashion-Mnist was chosen as the testing dataset, which includes ten classes of daily outfits. All the simulations used the backpropagation algorithm to update the connected weights in the neural network. In the simulation of the hardware-softplus neuron function, we take them into the hidden layer and the output layer, the activation of which was applied a softmax followed by a logarithm. Besides, in the simulation of the filtering unit, we added the softplus-like function before the input layer, with other structures unchanged.

Acknowledgements

This work was supported by the National Natural Science Foundation of China (61925401, 92064004, 61927901, 92164302) and the 111 Project (B18001). Y.Y. acknowledges support from the Fok Ying-Tong Education Foundation and the Tencent Foundation through the XPLORER PRIZE.

References

- [1] K. He, X. Zhang, S. Ren, J. Sun, presented at *Proceedings of the IEEE conference on computer vision and pattern recognition* ,**2016** .
- [2] F. Zhou, Z. Zhou, J. Chen, T. H. Choy, J. Wang, N. Zhang, Z. Lin, S. Yu, J. Kang, H.-S. P. J. N. n. Wong, *Nat. Nanotechnol.***2019** , *14* , 776.
- [3] K. Liu, T. Zhang, B. Dang, L. Bao, L. Xu, C. Cheng, Z. Yang, R. Huang, Y. Yang, *Nat. Electron.* **2022** , *5* , 761.
- [4] A. Sebastian, M. Le Gallo, R. Khaddam-Aljameh, E. Eleftheriou, *Nat. Nanotechnol.* **2020** , *15* , 529.

- [5] C. Choi, J. Leem, M. Kim, A. Taqieddin, C. Cho, K. W. Cho, G. J. Lee, H. Seung, H. J. Bae, Y. M. Song, T. Hyeon, N. R. Aluru, S. Nam, D.-H. Kim, *Nat. Commun.* **2020** , *11* , 5934.
- [6] P. Yao, H. Wu, B. Gao, J. Tang, Q. Zhang, W. Zhang, J. J. Yang, H. Qian, *Nature* **2020** , *577* , 641.
- [7] M. A. Zidan, J. P. Strachan, W. D. J. N. e. Lu, *Nat. Electron.* **2018** , *1* , 22.
- [8] M. Prezioso, F. Merrih-Bayat, B. D. Hoskins, G. C. Adam, K. K. Likharev, D. B. Strukov, *Nature* **2015** , *521* , 61.
- [9] S. Pi, C. Li, H. Jiang, W. Xia, H. Xin, J. J. Yang, Q. Xia, *Nat. Nanotechnol.* **2018** , *14* , 35.
- [10] B. Dang, K. Liu, X. Wu, Z. Yang, L. Xu, Y. Yang, R. Huang, *Adv. Mater.* **2022** , 2204844.
- [11] R. Cao, X. Zhang, S. Liu, J. Lu, Y. Wang, H. Jiang, Y. Yang, Y. Sun, W. Wei, J. Wang, H. Xu, Q. Li, Q. Liu, *Nat. Commun.* **2022** , *13* , 7018.
- [12] H. Lee, S. W. Cho, S. J. Kim, J. Lee, K. S. Kim, I. Kim, J.-K. Park, J. Y. Kwak, J. Kim, J. Park, Y. Jeong, G. W. Hwang, K.-S. Lee, D. Ielmini, S. Lee, *Nano Lett.* **2022** , *22* , 733.
- [13] S. Oh, Y. Shi, J. del Valle, P. Salev, Y. Lu, Z. Huang, Y. Kalcheim, I. K. Schuller, D. Kuzum, *Nat. Nanotechnol.* **2021** , *16* , 680.
- [14] X. Yan, J. Ma, T. Wu, A. Zhang, J. Wu, M. Chin, Z. Zhang, M. Dubey, W. Wu, M. S.-W. Chen, J. Guo, H. Wang, *Nat. Commun.* **2021** , *12* , 5710.
- [15] Q. Duan, Z. Jing, X. Zou, Y. Wang, K. Yang, T. Zhang, S. Wu, R. Huang, Y. J. N. c. Yang, *Nat. Commun.* **2020** , *11* , 3399.
- [16] Q. Duan, T. Zhang, C. Liu, R. Yuan, G. Li, P. Jun Tiw, K. Yang, C. Ge, Y. Yang, R. Huang, *Adv. Intell. Syst.* **2022** , *4* , 2200039.
- [17] Q. Wu, B. Dang, C. Lu, G. Xu, G. Yang, J. Wang, X. Chuai, N. Lu, D. Geng, H. Wang, L. Li, *Nano Lett.* **2020** , *20* , 8015.
- [18] M. D. Pickett, G. Medeiros-Ribeiro, R. S. Williams, *Nat. Mater.* **2012** , *12* , 114.
- [19] R. Yuan, Q. Duan, P. J. Tiw, G. Li, Z. Xiao, Z. Jing, K. Yang, C. Liu, C. Ge, R. Huang, Y. Yang, *Nat. Commun.* **2022** , *13* , 3973.
- [20] Z. Wang, M. Rao, R. Midya, S. Joshi, H. Jiang, P. Lin, W. Song, S. Asapu, Y. Zhuo, C. Li, H. Wu, Q. Xia, J. J. Yang, *Adv. Funct. Mater.* **2017** , *28* .
- [21] Z. Wang, S. Joshi, S. Savel'ev, W. Song, R. Midya, Y. Li, M. Rao, P. Yan, S. Asapu, Y. Zhuo, H. Jiang, P. Lin, C. Li, J. H. Yoon, N. K. Upadhyay, J. Zhang, M. Hu, J. P. Strachan, M. Barnell, Q. Wu, H. Wu, R. S. Williams, Q. Xia, J. J. Yang, *Nat. Electron.* **2018** , *1* , 137.
- [22] T. Tuma, A. Pantazi, M. Le Gallo, A. Sebastian, E. J. N. n. Eleftheriou, *Nat. Nanotechnol.* **2016** , *11* , 693.
- [23] Y. Fu, Y. Zhou, X. Huang, B. Dong, F. Zhuge, Y. Li, Y. He, Y. Chai, X. Miao, *Adv. Funct. Mater.* **2022** , *32* , 2111996.
- [24] H.-T. Zhang, T. J. Park, A. N. Islam, D. S. Tran, S. Manna, Q. Wang, S. Mondal, H. Yu, S. Banik, S. J. S. Cheng, *Science* **2022** , *375* , 533.
- [25] L. Xu, J. Zhu, B. Chen, Z. Yang, K. Liu, B. Dang, T. Zhang, Y. Yang, R. Huang, *Nat. Commun.* **2022** , *13* , 4698.
- [26] X. Zhu, D. Li, X. Liang, W. D. Lu, *Nat. Mater.* **2018** , *18* , 141.
- [27] X. Wan, T. Tsuruoka, K. Terabe, *Nano Lett.* **2021** , *21* , 7938.

- [28] Y. van de Burgt, E. Lubberman, E. J. Fuller, S. T. Keene, G. C. Faria, S. Agarwal, M. J. Marinella, A. Alec Talin, A. Salleo, *Nat. Mater.* **2017** , *16* , 414.
- [29] Y. Li, E. J. Fuller, J. D. Sugar, S. Yoo, D. S. Ashby, C. H. Bennett, R. D. Horton, M. S. Bartsch, M. J. Marinella, W. D. Lu, A. A. Talin, *Adv. Mater.* **2020** , *32* , 2003984.
- [30] H. Wei, R. Shi, L. Sun, H. Yu, J. Gong, C. Liu, Z. Xu, Y. Ni, J. Xu, W. Xu, *Nat. Commun.* **2021** , *12* , 1068.
- [31] J. Xue, Z. Zhu, X. Xu, Y. Gu, S. Wang, L. Xu, Y. Zou, J. Song, H. Zeng, Q. J. N. l. Chen, *Nat. Mater.* **2018** , *18* , 7628.
- [32] J. R. Treicher, *IEEE Trans. Acoust., Speech Signal Process.* **1983** , *31* , 349.
- [33] Y. Li, Z. Xuan, J. Lu, Z. Wang, X. Zhang, Z. Wu, Y. Wang, H. Xu, C. Dou, Y. Kang, Q. Liu, H. Lv, D. Shang, *Adv. Funct. Mater.* **2021** , *31* , 2100042.
- [34] Y. Li, H. Xu, J. Lu, Z. Wu, S. Wu, X. Zhang, Q. Liu, D. Shang, *Appl. Phys. Lett.* **2022** , *120* , 021901.
- [35] Y. Li, J. Lu, D. Shang, Q. Liu, S. Wu, Z. Wu, X. Zhang, J. Yang, Z. Wang, H. Lv, M. Liu, *Adv. Mater.* **2020** , *32* , 2003018.
- [36] H. Xu, R. Fang, S. Wu, J. An, W. Zhang, C. Li, J. Lu, Y. Li, X. Xu, Y. Wang, Q. Liu, D. Shang, *Adv. Electron. Mater.* **2022** , 2200915.
- [37] R. Yuan, M. Ma, L. Xu, Z. Zhu, Q. Duan, T. Zhang, Y. Zhu, Y. Wang, R. Huang, Y. Yang, *Sci. China Infor. Sci.* **2020** , *63* , 202401.